Microstructure Characterization of ODS-RAFM Steels.

Journal:	*2008 MRS Fall Meeting*
Manuscript ID:	1125-R05-03.R2
Symposium:	Symposium R
Date Submitted by the Author:	16-Apr-2009
Complete List of Authors:	Mateus, Rodrigo; Instituto Superior Técnico, Euratom/IST, Instituto de Plasmas e Fusão Nuclear Carvalho, Patrícia; Instituto Superior Técnico, Euratom/IST, Instituto de Plasmas e Fusão Nuclear Nunes, Daniela; Instituto Superior Técnico, Euratom/IST, Instituto de Plasmas e Fusão Nuclear Alves, Luís; Instituto Tecnológico e Nuclear, Departamento de Física Franco, Nuno; Instituto Tecnológico e Nuclear, Departamento de Física Correia, José; LNEG, Departamento de Materiais e Tecnologias de Produção Fernandes, Horácio; Instituto Superior Técnico, Euratom/IST, Instituto de Plasmas e Fusão Nuclear Silva, Carlos; Euratom/IST, Instituto de Plasmas e Fusão Nuclear, Instituto Superior Técnico Alves, Eduardo; Instituto Tecnológico e Nuclear, Departamento de Física Lindau, Rainer; Forschungszentrum Karlsruhe, Institut für Materialforchung I
Keywords:	nuclear materials, oxide, microstructure

Microstructure characterization of ODS-RAFM steels

R. Mateus[1], P.A. Carvalho[1,2], D. Nunes[1,2], L.C. Alves[3], N. Franco[3], J.B. Correia[4], H. Fernandes[1], C. Silva[1], R.Lindau[5], E. Alves[3]

[1]Associação Euratom/IST, Instituto de Plasmas e Fusão Nuclear, Instituto Superior Técnico, Av. Rovisco Pais, 1049-001 Lisboa, Portugal
[2]ICEMS, Departamento de Engenharia de Materiais, Instituto Superior Técnico, Av. Rovisco Pais, 1049-001 Lisboa, Portugal
[3]ITN, Instituto Tecnológico e Nuclear, Estrada Nacional 10, 2686-953 Sacavém, Portugal
[4]LNEG, Departamento de Materiais e Tecnologias de Produção, Estrada do Paço do Lumiar, 1649-038 Lisboa, Portugal
[5]FZK, Institut für Materialforchung I, PO Box 3640, 76021, Karlsruhe, Germany

ABSTRACT

Results of the microstructural characterization of four different RAFM ODS Eurofer 97 batches are presented and discussed. Analyses and observations were performed by nuclear microprobe and scanning and transmission electron microscopy. X-ray elemental distribution maps obtained with proton beam scans showed homogeneous composition within the proton beam spatial resolution and, in particular, pointed to a uniform distribution of ODS (yttria) nanoparticles in the Eurofer 97 matrix. This was confirmed by transmission electron microscopy. Scanning electron microscopy coupled with energy dispersive spectroscopy made evident the presence of chromium carbide precipitation. Precipitates occurred preferentially along grain boundaries (GB) in three of the batches and presented a discrete distribution in the other, as a result of different thermo-mechanical routes. Additional electron backscattered diffraction experiments revealed the crystalline textures in the ferritic polycrystalline structure of the ODS steel samples.

INTRODUCTION

An imperative property of materials suitable for fusion applications is low neutron activation. In order to comply with this requisite, reduced activation ferritic/martensitic (RAFM) Eurofer 97 steel has been developed from the conventional 9Cr-1Mo composition [1]. The substitution of high activation elements (Mo and Nb) by low activation chemically equivalent elements (W, V and Ta) resulted in a material that additionally evidences high swelling and creep resistances, as well as suitable tensile strength up to a temperature of 550 ºC [2-4]. The subsequently developed oxide dispersion strengthened (ODS) Eurofer 97 represents an increase in operation temperature to 650 ºC [5]. Furthermore, nanoparticle dispersions minimize radiation induced defects and improve the thermal stability of the material [6,7]. One of the most promising ODS oxides for fusion applications is Y_2O_3 which should be homogeneously distributed over the matrix for an optimum effect [5,8]. Yet, ODS Eurofer 97 presents still an unsatisfactory impact resistance and a to high ductile-to-brittle transition temperature [5]. Recent investigations indicate that these shortcomings may be obviated by suitable thermo-mechanical processing routes [9].

"First generation ODS Eurofer 97 steels" have been previously produced by mechanical alloying (MA) followed by standard hot isostatic pressure (HIP). However, this processing route originated inconvenient carbide film precipitation along GBs [9]. To overcome this shortcoming subsequent thermo-mechanical treatments have been introduced in the processing route of "second generation ODS Eurofer 97 steels", which induce discrete carbide precipitation [9].

Microstructural characterization of four Y_2O_3 Eurofer 97 batches have been studied at IST/ITN. This work presents preliminary results obtained with μ-Proton Induced X-ray Analysis (μ-PIXE), Scanning Electron Microscopy (SEM), Energy Dispersive X-ray Spectroscopy (EDS), Electron Backscattered Diffraction (EBSD) and Transmission Electron Microscopy (TEM).

EXPERIMENT

The production of the ODS RAFM steels resulted from a collaboration between PLANSEE and the FZK Institute of Karlsruhe. The basic idea was to fabricate near-net-shape blanket structures of "second generation" ODS RAFM steel [9]. Inert-gas-atomized RAFM Eurofer 97 steel powder was mechanically alloyed with 0.3 wt.% Y_2O_3 powder under an inert atmosphere. The resulting material was consolidated by HIP at 1150 ºC and 100 MPa, during 2 h [9]. Subsequently, plates with 16 and 6 mm of thickness (designated hereafter as Plate 16 and Plate 6, respectively) were produced via a hot rolling process, and rods with diameters of 20 and 12.5 mm (designated hereafter as Rod 20 and Rod 12.5, respectively) were produced by rotary swaging (Rod 20) and hot extrusion (Rod 12.5). These ODS RAFM materials were sent to IST/ITN for subsequent investigation.

Scanning nuclear microprobe investigations have been carried out with a Oxford Microbeam instrument using 2.0 MeV proton beams of ~3x3 μm^2. Cr and Fe distribution maps were obtained with currents close to 100 pA and a 50μm Mylar filter in front of the Si(Li) detector. Due to the low concentration of W and Y, their maps were obtained with a current close to 1 nA using a mixed filter consisting of a 125μm Mylar layer, 300μm Al foils and a 1 mm Perspex absorber.

SEM experiments were preformed with a JEOL 7001F field-emission gun equipped for EDS and EBSD. Accelerating voltages of 15 kV were used both for imaging and EDS analysis. Samples were initially prepared with mirror quality polishing (3 μm diamond spray grade) and etched with Vilella's reagent. Vilella's was sub-optimal in revealing grain contour, as it induced severely differentiated grain attack depending on specific crystallographic orientations. Grain size and morphology evaluation was refined with EBSD experiments, which enabled also to determine the preferential crystallographic orientations (textures) in the materials. EBSD experiments were carried out at 20 kV. Sample preparation implicated an additional polishing step performed with a suspension of 0.05 μm colloidal silica particles.

TEM observations have been performed with a Hitachi H8100 microscope equipped for EDS. The sample preparation involved cutting a disc with a diameter of 3 mm, and grinding until a thickness of 80 μm was reached. The samples were thinned to electron transparency by argon ion milling using a Gatan-Duo Mill machine operated at an acceleration voltage of 4 kV, with a 14^o incident angle.

RESULTS AND DISCUSSION

Inhomogeneities affect the final properties of the material [8,10] and can be avoided with convenient control of the processing parameters. Elemental distribution maps obtained from nuclear microprobe proton beam scans are becoming a standard and efficient technique for detection of macrosegregation and/or contamination in ODS RAFM steels [10]. The technique also allows evaluating the homogeneity of oxide particle distributions in the matrix [8]. In the present work the nuclear microprobe maps did not reveal any elemental contrast and point to a uniform distributionof all the elements constituting the ODS Eurofer 97 within the spatial resolution of the nuclear microprobe,. In particular, the Y signal demonstrates a homogeneous distribution of yttria. As an example, figure 1 shows the maps related to the presence of Cr, Fe, W and Y in Plate 16. Integral μ-PIXE spectra revealed a mean composition within the standard concentration range of Eurofer 97 [11] and a Y_2O_3 content of about 0.26 wt.% in all the batches. μ-PIXE results related to the distribution maps of figure 1 are presented in table 1.

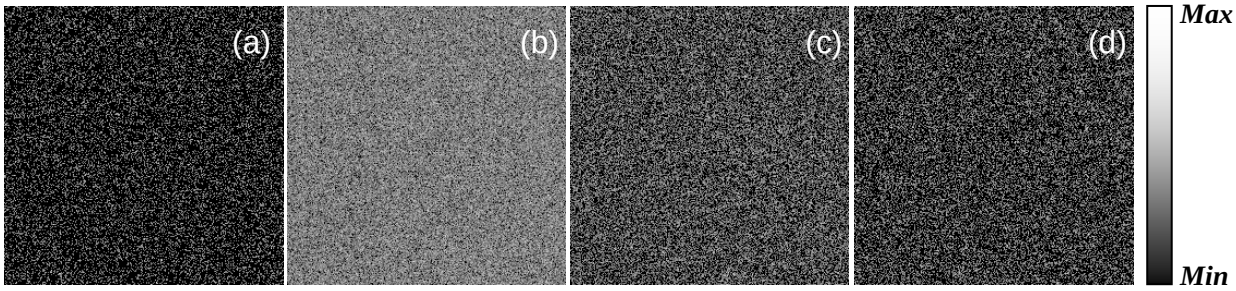

Figure 1. Distribution elemental maps of Plate 16 obtained from (a) Cr, (b) Fe, (c) W and (d) Y K_α lines with 75x75 μm^2 proton beam scans. The contrast difference between each map depends on the accumulation conditions and is not a measure of the relative element concentration. No contrast difference can be detected within each map.

Table 1.
Cr, Fe, W and Y_2O_3 content in Plate 16 (wt.%) obtained by μ-PIXE.

Cr	Fe	W	Y_2O_3
9.30±0.09	88.54±0.89	1.12±0.03	0.25±0.02

SEM observations revealed different precipitation morphologies in the batches. Figure 2 (a) shows discrete precipitates in the microstructure of Plate 16. In opposition, figure 2 (b) shows the typical precipitate morphology and distribution observed in Plate 6, Rod 20 and Rod 12.5: preferential film precipitation along GBs. The discrete precipitates diameter and film thickness were in the 50-100 μm range. EDS spectra revealed a Cr (and also W) enrichment in both types of precipitates in association with enhanced C content (as compared with the matrix), demonstrating chromium carbide presence. These results are in agreement with previous electron diffraction work, where the presence of $M_{23}C_6$ carbide was established [12]. Figure 2 (c) presents a TEM image obtained from Plate 16 demonstrating a fairly uniform distribution of ODS nanoparticles. Since the thermo-mechanical treatments were carried out above the solvus temperature [13], the microstructures indicate that carbide films formed during cooling from the hot rolling, hot extrusion and rotary swaging operations corresponding to the processing routes

of Plate 6, Rod 20 and Rod 12.5, respectively. The globular carbides in Plate 16 suggest an austenization treatment followed by tempering after hot-rolling.

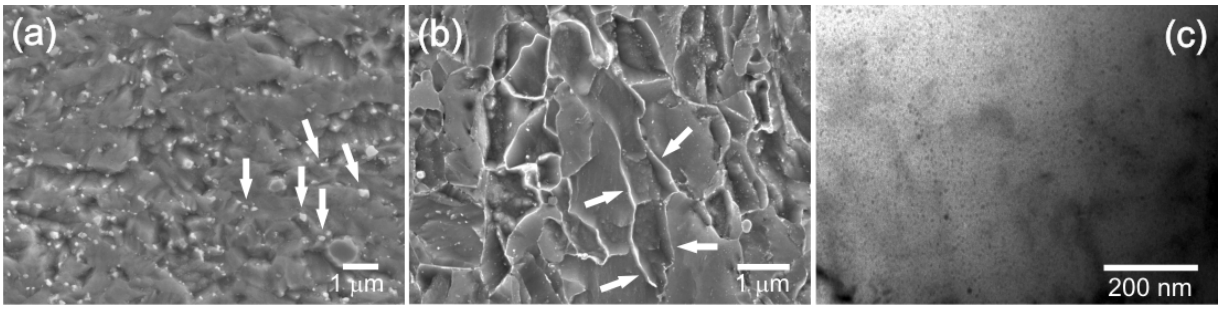

Figure 2. (a) Discrete carbide precipitatites in Plate 16; (b) carbide film along GBs in Plate 6, Rod 20 and Rod 12.5; (c) yttria nanoparticles spread observed along the Eurofer 97 matrix of Plate 16.

EBSD allowed determining an average grain size of about 1 µm and a ferritic structure in about 90% of the polished surfaces for all the batches. The non identified material was essentially associated with grain boundary structures and/or precipitates (see figure 3). All the conditions showed preferential crystallographic orientations. As an example, figure 4 presents <100>, <110> and <111> pole figures obtained from EBSD maps of transverse cross sections of Rod 20 and Rod 12.5, which reveal a complex texture for the swaged material (Rod 20) and a strong fiber texture for the extruded material (Rod 12.5).

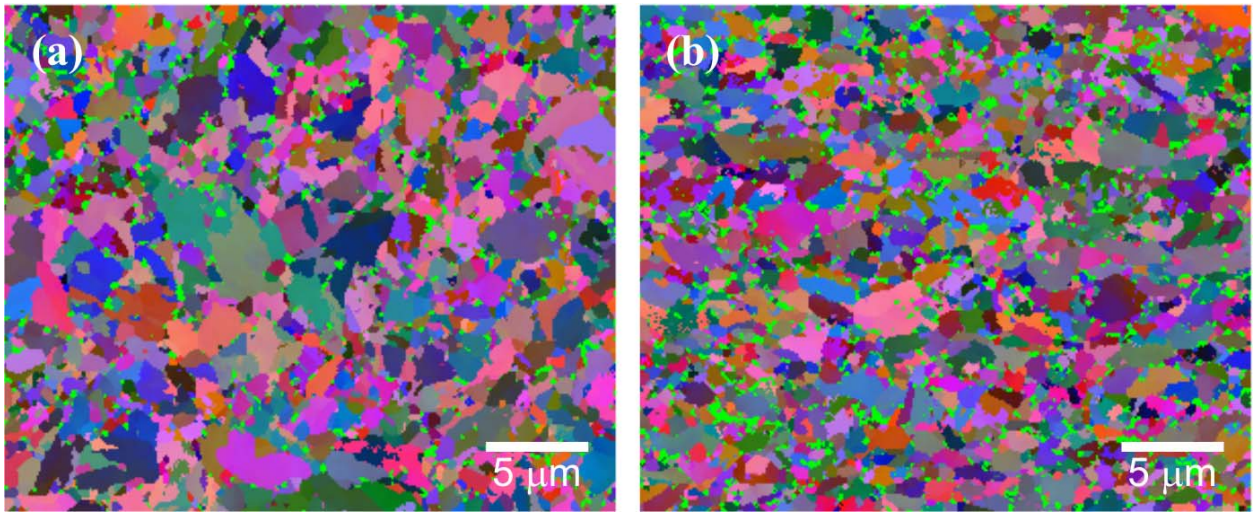

Figure 3. EBSD maps obtained from transverse cross sections of Rod 20 (a) and Rod 12.5 (b). The light green patches correspond to non identified material which is essentially associated with grain boundary structures and/or precipitates.

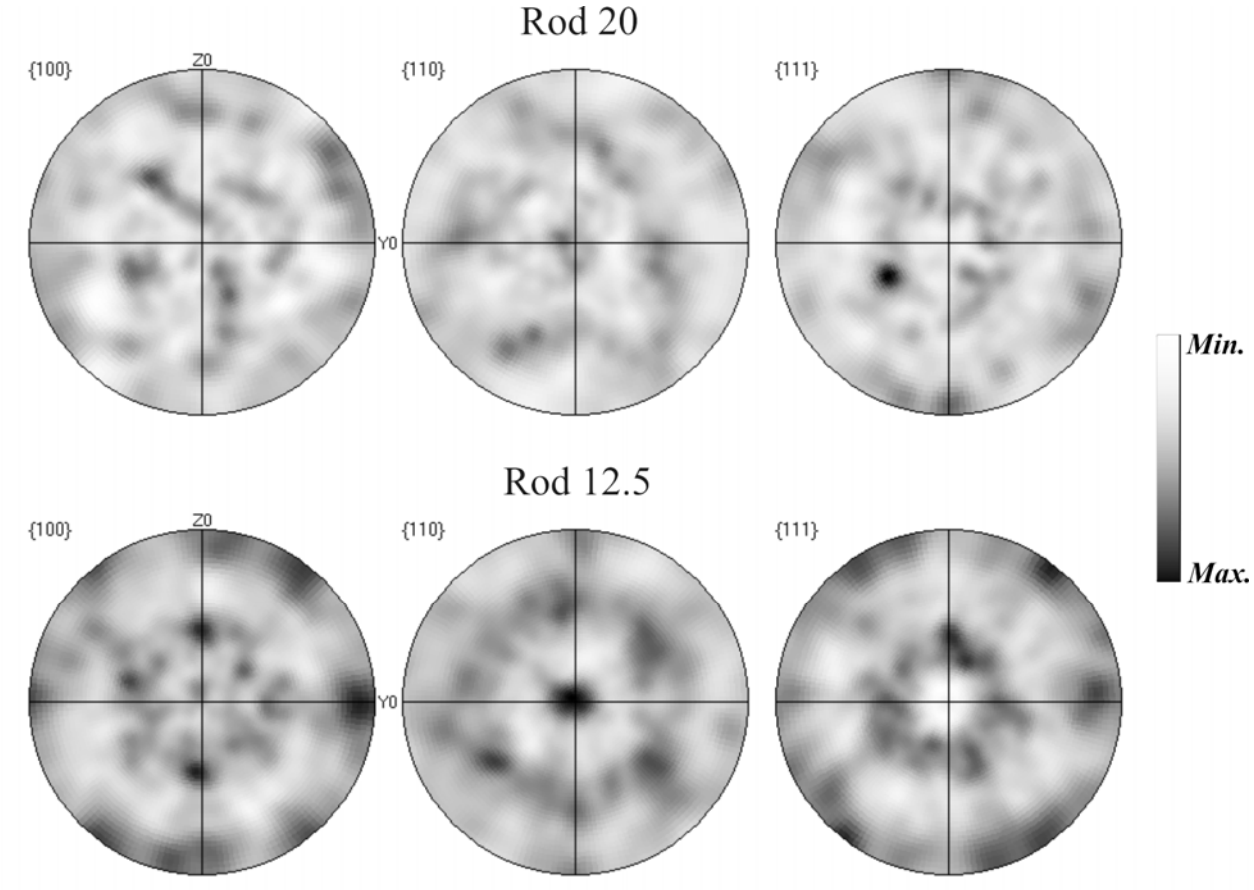

Figure 4. Pole figures obtained from EBSD maps of Rod 20 (top) and Rod 12.5 (bottom).

CONCLUSIONS

Elemental distribution maps showed homogenous chemical composition within the spatial resolution of the nuclear microprobe. TEM results pointed to a uniform distribution of ODS particles across the matrix. The ODS Eurofer microstructures reflected the thermo-mechanical route of each batch production, which resulted in chromium carbide film precipitation along GBs (Plate 6, Rod 20 and Rod 12.5) and in discrete chromium carbide precipitation (Plate 16). The thermo-mechanical processing routes induced strong textures in the materials.

ACKNOWLEDGMENTS

This work has been carried out within the Contract of Association between EURATOM and Instituto Superior Técnico. Financial support was also received from Fundação para a Ciência e Tecnologia in the frame of the Associated Laboratory Contract.

REFERENCES

1 J. Waering, A.-A.F. Tavassoli, Assessment of Martensitic Steels for Advanced Fusion Reactors, in: S.V. Moller, J.D Riera, (Eds.), Transactions of the 13th International Conference in

Structural Mechanics in Reactor Technology, Porto Alegre, Brazil, Universidade Federal do Rio Grande do Sul (UFRGS), 13-18 Agust 1995, Division E, p.563.
2. N. Baluc, K. Abe, J.L. Boutard, V.M. Chernov, E. Diegele, S. Jitsukawa, A. Kimura, R.L. Klueh, A. Kohyama, R.J. Kurtz, R. Lässer, H. Matsui, A. Möslang, T. Muroga, G.R. Odette, M.Q. Tran, B. van der Schaaf, Y. Wu, J. Yu,S.J. Zinkle, Nucl. Fusion 47, S696 (2007).
3. N. Baluc, D.S. Gelles, S. Jitsukawa, A. Kimura, R.L. Klueh, G.R. Odette, B. van der Schaaf and Jinnan Yu, J. Nucl. Mater. 367-370, 33 (2007).
4. S. Ukai, M. Fujiwara, J. Nucl. Mater. 307-311, 749 (2002).
5. R. Lindau, A. Möslang, M. Schirra, P. Schlossmacher, M. Klimenkov, J. Nucl. Mater. 307-311, 769 (2002).
6 M.S. El-Genk, J.M. Tournier, J. Nucl. Mater. 340 (2005) 93.
7. T. Hayashi, P.M. Sarosi, J.H. Schneibel, M.J. Mills, Acta Mater. 56, 1407 (2008).
8. A. Paúl, E. Alves, L.C. Alves, C. Marques, R. Lindau, J.A. Odriozola, Fusion Eng. Des. 75-79, 1061 (2005).
9. M. Klimenkov, R. Lindau, A. Möslang, J. Nucl. Mater. 367-370, 173 (2007).
10. L.C. Alves, E. Alves, A. Paúl, M.R. da Silva, J. A. Odriozola, Nucl. Instr. and Meth. B 249, 493 (2006).
11. A.-A.F. Tavassoli, A. Alamo, L. Bedel, L. Forest, J.-M. Gentzbittel, J.-W. Rensman, E. Diegele, R. Lindau, M. Schirra, R. Schmitt, H.C. Schneider, C. Petersen, A.-M. Lancha, P. Fernandez, G. Filacchioni, M.F. Maday, K. Mergia, N. Boukos, N. Baluc, P. Spätig, E. Alves, E. Lucon, J. Nucl. Mater. 329-333, 257 (2004).
12. A. Paúl, A. Beirante, N. Franco, E. Alves, J.A. Odriozola, Mater. Science Forum, 514-516, 500 (2006).
13. R. Lindau, M. Schirra, Fusion Eng. Des. 58–59, 781 (2001).